New Directions in Geosciences
for Unconventional Resources

OCTOBER 15-17, 2019
BANFF, CANADA

William C. Gussow GEOSCIENCE CONFERENCE
CSPG

A Tale of Three Earthquakes: New Insights into Fault Activation in Light of Recent Occurrences in Western Canada

David W. Eaton*[1], Alireza Mahani[2], Rebecca Salvage[1], Honn Kao[3] and Mirko van der Baan[4];
1. Department of Geoscience, University of Calgary, 2. Mahan Geophysical Consulting Inc.,
3. Natural Resources Canada, 4. Department of Physics, University of Alberta

Abstract

Earthquakes large enough to be widely felt at the surface have occurred, albeit rarely, during or shortly after hydraulic-fracturing operations for development of unconventional hydrocarbon resources. In recent years, the issue of injection-induced earthquakes has received considerable public attention in areas such as the U.S. midwest, where the primary triggering mechanism is generally due to large-volume disposal of co-produced brines. In Canada, regulatory issues have come into sharper focus due to a recent earthquake sequence near Fort St. John, BC and several felt events west of Red Deer, Alberta. These events are currently under investigation to better understand ground shaking, aftershock productivity, source mechanisms, fault architecture and local stress environment. New models are being developed suggesting that the physical process of fault activation is not as straightforward as previously envisioned models that invoke only an increase in pore-pressure in the seismogenic region.

Introduction

Although the vast majority of hydraulic-fracturing well completions do not generate felt seismicity, in rare cases anomalous induced events have been triggered by hydraulic fracturing (Eaton, 2018). Documented occurrences of hydraulic-fracturing induced events have taken place in western Canada (Atkinson et al., 2016; Bao and Eaton, 2016; Mahani et al, 2017), Ohio (Skoumal et al., 2015), the United Kingdom (Clarke et al., 2014) and China (Lei et al., 2019). Similarly, a dramatic increase in injection-induced seismicity has also taken place in the U.S. midwest region, including Oklahoma, but the primary triggering mechanism for events in this region is different – namely, large-volume disposal of co-produced brines rather than hydraulic fracturing well completions (Ellsworth, 2013; Rubinstein and Mahani, 2015). In general, the occurrence of felt events due to fluid injection are thought to require the existence of an injection source, a pathway that connects fluid pressure or stress perturbation from the source to the seismogenic region, and a fault that is capable of hosting a sufficiently large earthquake (Gallis et al, 2017; Eaton and Igonin, 2018; Eaton, 2018). Fault activation by hydraulic fracturing is commonly attributed to an increase in pore pressure, but it may also be triggered by poroelastic stress transfer or fault loading due to aseismic creep (Bourouis and Bernard, 2007; Ellsworth, 2013; Bao and Eaton, 2016; Schultz et al., 2017; De Barros et al, 2019; Bhattacharya and Viesca, 2019).

In response to increased recognition of risks of injection-induced seismicity from hydraulic fracturing, the Alberta Energy Regulator (AER) implemented an Induced-Seismicity Traffic-Light Protocol (IS-TLP) for the Kaybob-Duvernay Monitoring Area (Figure 1) near Fox Creek, AB (AER, 2015). This protocol requires oil and gas operators to report any occurrence of a seismic event of local magnitude (M_L) between 2.0 and 4.0 (amber light) within 5 km of a hydraulic fracturing well, or to halt operations if a seismic event of M_L above 4.0 (red light) is detected within 5 km. Recently, partly in response to felt earthquakes in central Alberta, AER has recommended the use of a IS-TLP in the Red Deer Monitoring Area (AER, 2019). In 2016, the British Columbia Oil and Gas Commission (BCOGC) implemented requirements for ground-motion monitoring (BCOGC, 2016) based on local magnitude and peak ground acceleration (PGA) in two areas in northeast BC (Figure 1). The initial PGA reporting threshold of 2%g (1g = 9.8 m/s^2) was reduced to 0.8%g in 2018 (BCOGC, 2018).

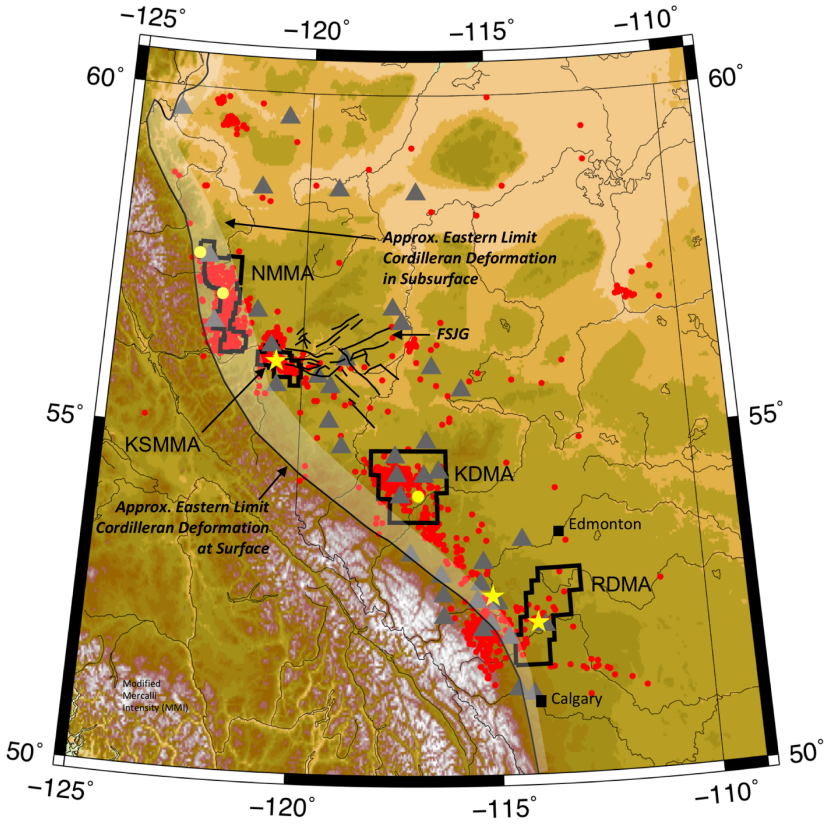

Figure 1: Map of historical seismicity (red dots) in the Western Canada Sedimentary Basin, with quarry blasts removed. Yellow symbols show events in Table 1; stars denote three most recent events. Grey triangles indicate stations with public data, used for event detection and template matching. Locations of faults in the Fort St. John Graben (FSJG) system are from Richards et al. (1990); eastern limit of Cordilleran deformation at surface is from Price (1990) and the approximate subsurface limit is inferred based on seismic interpretation. Areas where seismic monitoring is required or recommended are shown by black boxes. NMMA = northern Montney Monitoring Area, KSMMA = Kiskatinaw Seismic Monitoring and Mitigation Area, KDMA = Kaybob Duvernay Monitoring Area, RDMA = Red Deer monitoring area.

Methods for induced-seismicity hazard assessment are under development, largely based on existing probabilistic seismic hazard assessment (PSHA) approaches for characterizing hazards from natural seismicity (e.g., Atkinson et al., 2015; Petersen et al., 2017). The basic steps for PSHA analysis can be summarized as (Baker, 2008; Eaton, 2018): 1) identify earthquake source regions; 2) characterize magnitude-frequency relationships; 3) determine the distribution of source-receiver distances; 4) apply ground-motion prediction equations (GMPEs) (Boore and Atkinson, 2008; Campbell and Bozorgnia, 2014; Atkinson, 2015); and 5) determine seismic hazard curves using a probabilistic approach.

Aims and Objectives

Although the general topic of injection-induced seismicity has been intensely studied during the past 5 years, certain practical aspects remain unclear, including: 1) how to identify and map potentially seismogenic faults prior to activation; 2) defining best practices for traffic-light protocols in order to manage and mitigate risks of induced seismicity. Recent induced seismicity in western Canada provided a rich dataset to study these issues, including three felt earthquakes that have occurred since late 2018 (Table 1). Included in this list is a M_L 4.3 event that took place on 10 March, 2019, which has no presently inferred association with anthropogenic activity (e.g., hydraulic fracturing, saltwater disposal, or production-related depletion) and so could provide an important type example of a natural earthquake (R. Schultz, pers. comm., 2019).

In this paper, we compile data pertinent to these events in order to gain an improved understanding of processes of fault activation, as well as regional patterns of ground motion. This is a work-in-progress and we are continuing to compile and interpret new data from these recent events

Event ID	Date	Time (UTC)	Latitude	Longitude	M	M Type	Mw	D (km)	D Source
1	**2018/11/30**	**01:27:06**	**56.0456**	**-120.6925**	**4.5**	**Mw**	**4.6**	**1.1**	**Operator**
3	2018/11/30	02:15:00	56.0465	-120.6875	4.0	ML	4.0	1.8	Operator
221	2014/08/04	17:17:24	57.5640	-122.9420	4.5	Mw	4.7	5	Fixed
222	2015/06/13	23:57:55	54.1020	-116.9500	4.6	Mw	4.0	5	Fixed
265	2015/08/17	20:15:00	56.9894	-122.2350	4.6	Mw	4.7	2	Assumed
268	**2019/03/04**	**12:55:17**	**52.2200**	**-114.0700**	**4.6**	**ML**	**3.8**	**2**	**Assumed**
269	**2019/03/10**	**10:00:36**	**52.6200**	**-115.1400**	**4.3**	**ML**	**4.0**	**10**	**Fixed**

Table 1. Parameters of the earthquakes shown in Figure 1. M is the catalogue magnitude, M_L is the local magnitude, and M_W is the moment magnitude. Events in bold font represent three recent felt events that are a focus of this study. The column with the header Mw shows the values obtained using the method of Atkinson et al. (2014) as modified by Novakovic et al. (2018). The depth parameter (*D*) is used here for ground-motion analysis and may not reflect the actual focal depth of the earthquake.

Materials and Methods

Figure 1 shows historical seismicity (red dots) in the study region from the Composite Alberta Seismicity Catalog (https://www.inducedseismicity.ca/wp-content/uploads/2015/01/Composite-Alberta-Seismicity-Catalog3.pdf). This catalog is complete to the end of 2018/09 and includes data compiled semi-automatically from earthquake catalogs developed by different agencies. The pattern of seismicity in the raw catalog is spatially clustered, including concentrations of seismicity in areas of quarry blasting and induced seismicity. Events from known areas of quarry blasting have been removed in Figure 1 to highlight the main areas of induced seismicity. These areas mainly coincide with seismic monitoring areas outlined in Figure 1.

The moment magnitude (M_W) for each event in Table 1 was estimated from the vertical pseudo-response spectral acceleration (PSA) amplitudes obtain using the method of Atkinson et al. (2014), as modified by Novakovic et al. (2018) with coefficients for Oklahoma and Alberta. Stress drop in the range of 75-85 bars was obtained based on matching the observed PSA amplitudes with the GMPE obtained for Alberta (Novakovic et al., 2019).

Using public data from regional seismic monitoring networks (stations shown in Figure 1), downloaded from the Incorporated Research Institutes for Seismology (IRIS) portal, the Repeating Earthquake Detector (REDPy) algorithm developed by Hotovec-Eliis and Jeffries (2016) was employed to detect and characterize seismicity including aftershock productivity. REDPy uses a simple amplitude-ratio algorithm

with a coincident trigger on multiple stations to detect seismic events within a continuous data series. Here we use a long-term window of 3 seconds; a short-term window of 0.7 seconds; and a coincident trigger on at least 5 stations. Although the mainshocks, and several aftershocks were visible on public stations, no other seismic events could be clearly identified using a coincident trigger on at least 5 stations. This suggests that, in general, aftershocks were of too small a magnitude to be detected at the large distances of the public network.

REDPy was also applied to waveform data from a dense array private network near event 1 (Table 1). A total of 64 events were detected, from 27 November - 11 December (inclusive). The continuous data were first band-pass filtered between 1 and 40 Hz to remove very low-frequency noise that was evident in the waveforms. Of these 64 events, 16 were considered to have a high similarity (cross-correlation coefficient > 0.7) and could be divided into 6 families of events. The core event of each family (i.e., the event with the largest correlation coefficient with respect to all other events within a given family), as well as the events which did not correlate with any other events (orphans), were used as template signals using the EQCorrScan algorithm (Chamberlain et al., 2018). This method uses template matching to further populate the catalog with events which may have been previously missed by REDPy due to noise and/or temporal spacing. Template matching identified a total of 579 events, sorted into 42 families (> 3 events per family), with the largest family containing 161 events.

For all the events identified using EQCorrScan we calculated the root-mean-squared (RMS) amplitude, the frequency index (FI) and the inter-event time (IET). The Frequency Index (FI), developed by Buurman and West (2010), is a proxy for the spectral content of the waveform and is based upon the ratio of energy in low- and high-frequency windows, with a base-ten logarithm in order to reduce the index to a single value. A negative FI means the waveform is dominated by low-frequency energy, whereas a positive FI demonstrates that the majority of energy is in the high-frequency band. Here, we define the low-frequency window as 1 - 20 Hz, and the high frequency window between 20 - 40 Hz. The inter-event time presented here represents the time since the previous event, regardless of its family.

Results and Discussion

A number of regional tectonic elements are highlighted in Figure 1. These include the Rocky Mountain deformation front (as shown in Price, 1990), along with a foreland-extension of the thrust belt in the subsurface that is evident in industry seismic data. Recent felt earthquakes (yellow stars in Figure 1) occur close to this zone, consistent with observations of relatively higher present-day crustal strain (Kao et al., 2018). Another area of significant faulting is the Carboniferous-Permian Fort St. John Graben (FSJG), which intersects the Rocky Mountain deformation front near the location of event 1 (Figure 1). Apart from event 269, which may be of natural origin, all of the events in Table 1 are located within seismic monitoring regions defined by regulators including two within the BC Montney Play (Kiskatinaw Seismic Monitoring and Mitigation Area, Northern Montney Monitoring Area) and two within the Alberta Duvernay play (Kaybob Duvernay Monitoring Area, Red Deer Monitoring Area).

Figure 2 shows a graph of the horizontal component of PSA (RotD50; Boore, 2010) versus hypocentral distance for the events shown in Figure 1 and Table 1, at frequencies of 1.0, 3.3, 5.0, and 10.0 Hz. The observations generally agree with the GMPE of Novakovic et al. (2018) as modified by Babaie Mahani et al. (2019) for Alberta attenuation and plotted for events 1 and 3 (Table 1). Rodriguez-Pradilla and Eaton (2019) have also developed a new GMPE that includes a large number of near-source observations, for which the ground motion is less than predicted by this model. Babaie Mahani et al. (2019) analyzed the ground-motion amplitudes from the events occurred on November 30, 2018 in northeast BC. They found that stations within about 10 km of the hypocentre may have experienced nonlinear site response at high frequencies for the two largest events (events 1 and 3; Table 1). They also inferred that the value of stress drop for events 1 and 3 is approximately 50 bars, based on the agreement of observed PSA values with Novakovic et al. (2018) GMPE. For event 1, the peak ground acceleration was above the Modified Mercalli Intensity of VI at distances < 6 km, with strongest shaking occurring over a duration of 1.6 sec at the closest station located 3.5 km from the epicentre (Babaie Mahani et al., 2019).

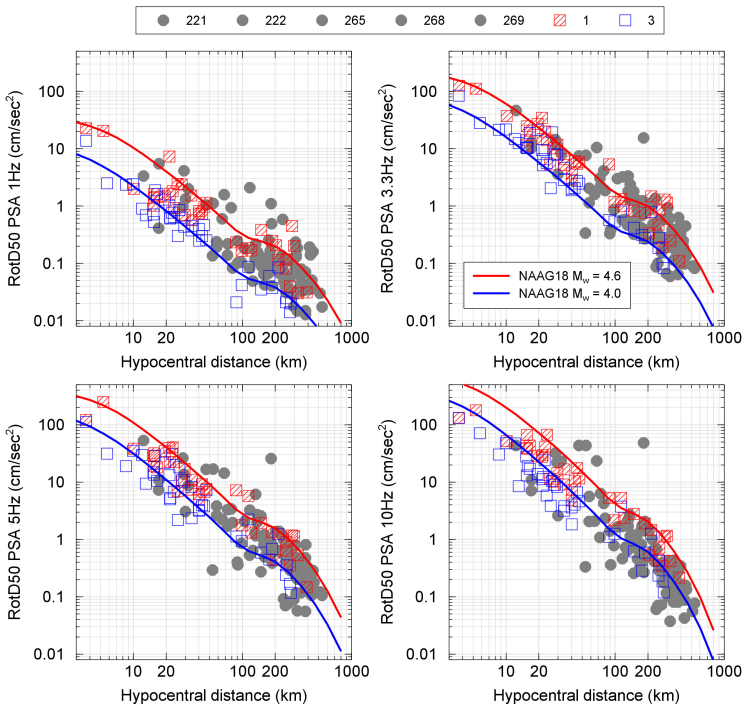

Figure 2: Pseudo-response spectral acceleration for the horizontal component (RotD50; Boore, 2010) versus hypocentral distance for the events shown in Figure 1 and Table 1 at frequencies 1, 3.3, 5, and 10 Hz. Solid lines are the estimated amplitudes from Novakovic et al. (2018; NAAG18) for MW of 4.6 (event 1) and 4.0 (event 2) for Vs30 = 760 m/s.

Figure 3 shows graphs of seismicity rate (hourly event count), RMS amplitude, inter-event time and Frequency Index for event 1 (Table 1), located near Fort St. John BC. These results were calculated using REDPy from data from the dense array local network. The red and green vertical lines indicate the time of the mainshock and largest aftershock, both of which are removed from the graphs for clarity. Aftershock sequences are marked by conspicuous vertical bands that are expressed in every parameter except the inter-event time.

We have undertaken additional analysis of the 2018/11/30 earthquake sequence near Fort St. John, BC. Figure 4 shows epicentres of M > 1.5 events as well as focal mechanism diagrams (beach balls) for the 12 largest events. Family analysis has been applied to separate these events into distinct clusters, as indicated by the colour used for each mechanism. The mainshock is displayed in green and represents a predominantly reverse mechanism, interpreted as a reverse-sense reactivation of the normal fault the forms the southern boundary of the FSJG. Other events exhibit a diverse range of focal mechanisms, including strike-slip and low-angle thrust faulting. This diversity of source type suggests that a complex fault system. It is likely that this region lies near the transition from strike-slip to reverse faulting regimes.

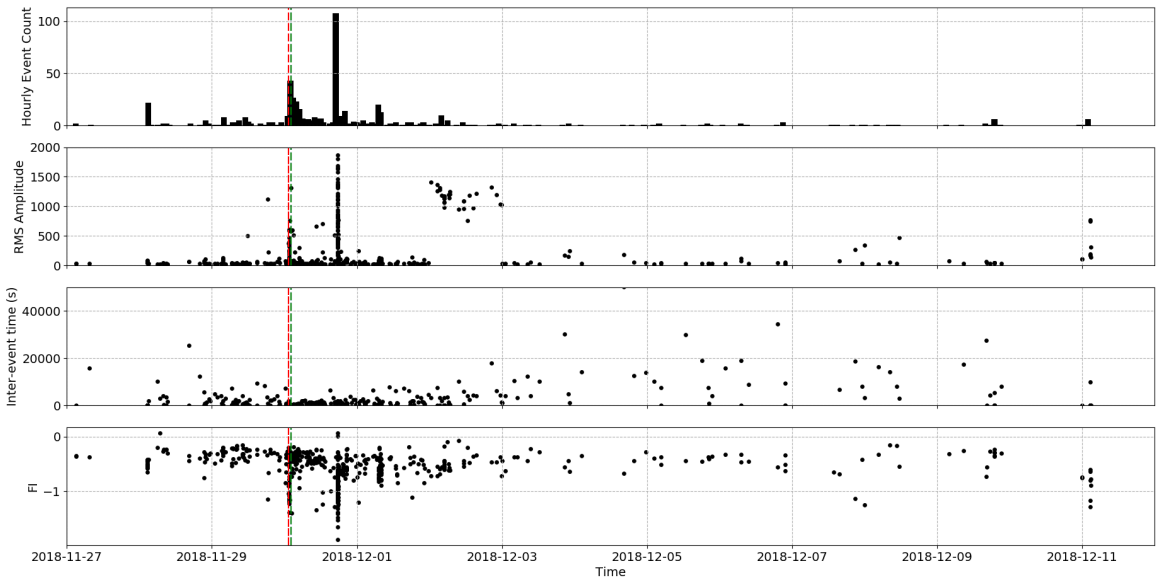

Figure 3: Repeating event detection analysis of waveform data from a dense array local network of 19 stations south of Fort St. John BC. The red and green dashed lines indicate the mainshock and largest aftershock of event 1 (Table 1), a M_W 4.5 earthquake on 2018/11/30. RMS = root-mean-square, FI = frequency index (see text).

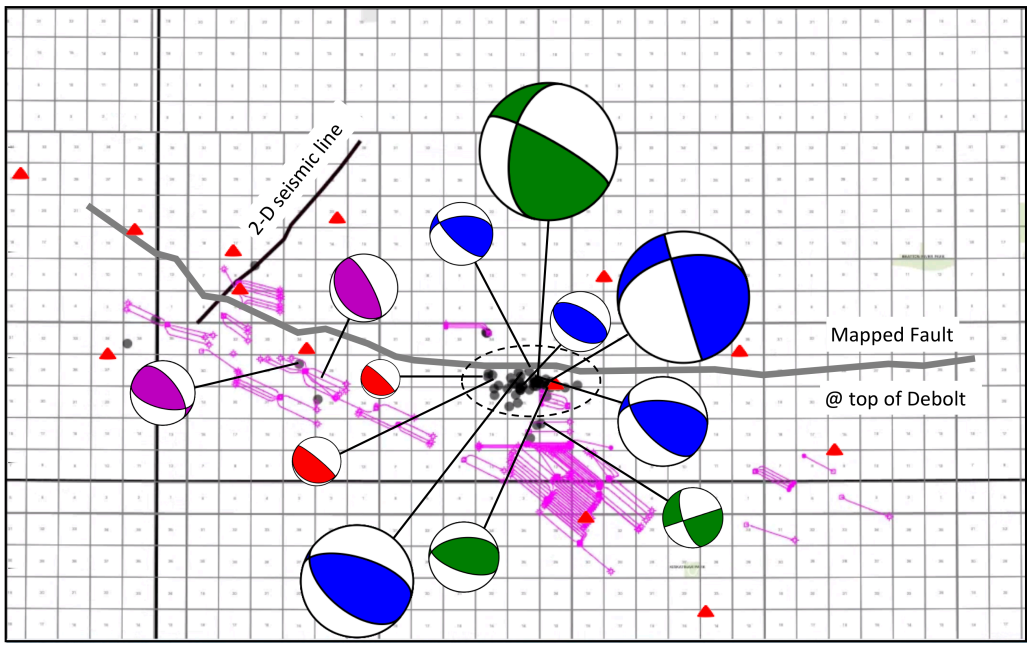

Figure 4: Map of the study area, showing: 1) horizontal wells (magenta lines) with diagnostic fracture injection test (DFIT) data used to measure minimum principal stress; 2) seismicity (grey dots) detected using a local industry seismograph array (red triangles), along with focal mechanisms used for stress inversion (scaled by magnitude); 3) location of the southern bounding fault of the Fort St. John Graben (FSJG), and 4) location of the 2-D seismic line in Fig. 5. Grey dots enclosed by the dashed ellipse show the distribution of aftershocks. Focal mechanisms were calculated by Nanometrics; corresponding beachball colours represent event clusters, determined as part of the focal-mechanism analysis. Seismicity data and waveforms were provided by ESG/Spectraseis. Small squares represent one section (1.6 x 1.6 km).

Based on the mapped trace of the fault at the level of the Debolt Formation, the southern bounding fault of the FSJG appears to consist of a series of discrete fault segments with varying orientation along strike. The distribution of aftershocks (grey dots enclosed within the dashed ellipse in Figure 4) suggests that the rupture dimensions of the slip area for this sequence may be bounded by locations where the orientation of the fault changes.

Figure 5 show a migrated 2-D seismic data (with and without fault interpretation) from a profile that crosses the southern boundary zone of the FSJG. A conservative interpretation of the fault structure derived from this seismic profile shows a step-wise northward transition into the main part of the graben. Individual faults appear to be listric and extend upwards to varying stratigraphic levels, possibly indicating variable geologic periods of fault activity along these Carboniferous-Permian structures. This profile shows that faults in this area are more clearly discernible using seismic data than the (mainly) vertical strike-slip faults in the Kaybob-Duvernay region (e.g. Eaton et al, 2018).

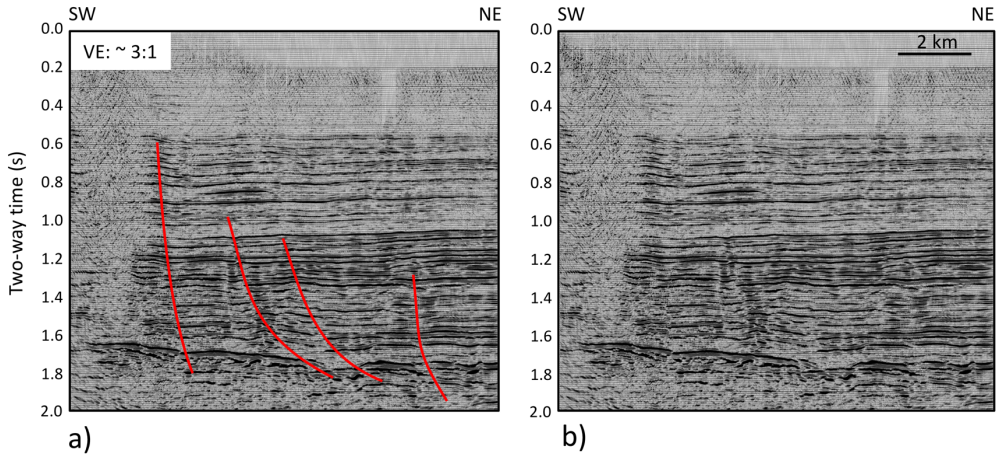

Figure 5: 2-D seismic profile (provided by Pulse Seismic Inc.) across the southern margin of the Fort St. John Graben; a) with, and b) without fault interpretation.

Future work

We are currently compiling data from dense array local network for events 268 and 269 (Table 1), which occurred very recently in March 2019. This additional data will allow us to undertake similar analysis using REDPy and EQCorrScan in order to create catalogs for these events. Comparisons of the amplitudes, frequency content, temporal and spatial evolutions of each of these earthquakes will likely render distinguishing properties of each of the sequences.

Once compilation has been completed, we plan to characterize the stress field by applying stress inversion using the method of Jia et al. (2018). The inferred stress field will enable us to test how the diverse focal mechanisms are linked to the stress regime. We will also apply risk analysis using an adaptation of the fault-slip potential software tool (Walsh and Zoback, 2016). This method uses a priori distributions of input parameters for stress state, fault geometry and frictional parameters, some of which are unusually well characterized due to the availability of industry data. Stochastic modelling of scenarios, compared with the Mohr-Coulomb failure criterion, will enable the slip potential of different fault segments (Figure 4) to be evaluated.

Conclusions

Three recent earthquakes in western Canada, on 2018/11/30 near Fort St. John, BC, on 2019/03/04 near Red Deer AB and on 2019/03/10 near Rocky Mountain House, AB provide new information that help to improve our knowledge of induced and natural seismicity in western Canada. We are currently compiling and analyzing information from these events, and this paper provides a brief progress report. Regional ground-motion data from these events are broadly consistent with the ground motion prediction equation of Novakovic et al. (2018) as modified by Babaie Mahani et al. (2019) for Alberta attenuation, assuming typical regional site amplification. In the case of the event near Fort St. John, peak ground acceleration exceeded Modified Mercalli Intensity of VI at distances < 6 km, with the strongest shaking occurring over a duration of 1.6 sec at the closest station located 3.5 km from the mainshock epicentre (Babaie Mahani et al., 2019). Stations within about 10 km of the mainshock may have experienced nonlinear site response at high frequencies. The combined use of a repeating signal detector (REDPy) and template matching will enable us to develop more complete seismicity catalogues for these events and thus to quantify aftershock productivity, especially in cases where we can access a dense array local seismograph network. Various measures such as inter-event time and frequency index will aid in grouping these events into specific families that have similar characteristics. The 2018/11/30 MW 4.5 earthquake reactivated a normal fault along the southern margin of the Fort St. John graben, with an oblique-reverse sense motion. This earthquake produced two felt aftershocks (ML 4.0 and ML 3.4). Subsequent events (including aftershocks) are characterized by a diversity of mechanisms, including reverse, strike-slip and low-angle thrusting. The fault appears to be segmented, and the earthquake sequence may be bounded between fault segments with varying orientation. In at least some instances, seismogenic faults in this area appear to be mappable using seismic-reflection profiles, in contrast to some other regions such as the Duvernay region in Alberta.

Acknowledgements

This project was undertaken as part of the Global Research Initiative in Sustainable Low Carbon Unconventional Resources at the University of Calgary, in part with support from the Canada First Research Excellence Fund (CFREF). Canadian Natural Resources Ltd. (CNRL), ESG/Spectraseis and Pulse Seismic are thanked for providing data used in this analysis. The focal mechanisms shown in Figure 4 were calculated by Nanometrics Ltd. and provided for this study by CNRL. Maps were produced using Generic Mapping Tools (GMT) and Petrel. Seismic waveform data were obtained from the archives of the Incorporated Research Institutions for Seismology (IRIS) and all of the original data contributors to this archive are sincerely thanked. Seismicity data in Figure 1 is from Composite Alberta Seismicity Catalogue (www.inducedseismicity.ca/catalogues).

References

Alberta Energy Regulator (AER), 2015. Subsurface Order #2, https://aer.ca/documents/orders/subsurface-orders/SO2.pdf

Alberta Energy Regulator (AER), 2019. Recommendations around Hydraulic Fracturing in the Red Deer Area. Bulletin 2019-07. https://www.aer.ca/documents/bulletins/Bulletin-2019-07.pdf

Atkinson, G.M., 2015. Ground-motion prediction equation for small-to-moderate events at short hypocentral distances, with application to induced-seismicity hazards. Bulletin of the Seismological Society of America, v. 105, p.981-992.

Atkinson, G. M., Greig, D.W., and Yenier, E. 2014. Estimation of moment magnitude (M) for small events (M < 4) on local networks, Seismological Research Letters, v. 85, p. 1116-1124.

Atkinson, G.M., Ghofrani, H. and Assatourians, K. 2015. Impact of induced seismicity on the evaluation of seismic hazard: Some preliminary considerations. Seismological Research Letters, v. 86, p.1009-1021.

Atkinson, G.M., Eaton, D.W., Ghofrani, H., Walker, D., Cheadle, B., Schultz, R., Shcherbakov, R., Tiampo, K., Gu, J., Harrington, R.M. and Liu, Y. 2016. Hydraulic fracturing and seismicity in the Western Canada Sedimentary Basin. Seismological Research Letters, v. 87, p.631-647.

Babaie Mahani, A. and Kao, H. 2018. Ground motion from M 1.5 to 3.8 induced earthquakes at hypocentral distance < 45 km in the Montney play of northeast British Columbia, Canada, Seismological Research Letters, v. 89, p. 22-34.

Baker, J.W., 2008. An introduction to probabilistic seismic hazard analysis (PSHA). White Paper, Version 1.3. https://web.stanford.edu/~bakerjw/Publications/Baker_(2008)_Intro_to_PSHA_v1_3.pdf

Bao, X. and Eaton, D.W. 2016. Fault activation by hydraulic fracturing in western Canada. Science, v. 354, p.1406-1409.

BC Oil and Gas Commission (BCOGC) (2016). Ground Motion Monitoring Requirements. Industry Bulletin 2016-19, https://www.bcogc.ca/node/13257/download.

BC Oil and Gas Commission (BCOGC) (2018). Kiskatinaw Seismic Monitoring and Mitigation Area Special Project Order. ORDER 18-90-001 (Amendment #1). https://www.bcogc.ca/node/14877/download

Bhattacharya, P. and Viesca, R.C. 2019. Fluid-induced aseismic fault slip outpaces pore-fluid migration. Science, v. 364, p.464-468.

Boore, D. M. and Atkinson, G. M. 2008. Ground-motion prediction equations for the average horizontal component of PGA, PGV, and 5%-damped PSA at spectral periods between 0.01 s and 10.0 s. Earthquake Spectra, v. 24, p.99-138.

Bourouis, S. and Bernard, P. 2007. Evidence for coupled seismic and aseismic fault slip during water injection in the geothermal site of Soultz (France), and implications for seismogenic transients. Geophysical Journal International, v. 169, p.723-732.

Buurman, H. and West, M.E. 2010. Seismic precursors to volcanic explosions during the 2006 eruption of Augustine Volcano: Chapter 2. In: The 2006 eruption of Augustine Volcano, Alaska (No. 1769-2, pp. 41-57). US Geological Survey.

Campbell, K.W. and Bozorgnia, Y., 2014. NGA-West2 ground motion model for the average horizontal components of PGA, PGV, and 5% damped linear acceleration response spectra. Earthquake Spectra, v. 30, p.1087-1115.

Chamberlain, C.J., Hopp, C.J., Boese, C.M., Warren-Smith, E., Chambers, D., Chu, S.X., Michailos, K. and Townend, J. 2018. EQcorrscan: Repeating and near-repeating earthquake detection and analysis in python. Seismological Research Letters, v. 89, p.173-181.

Clarke, H., Eisner, L., Styles, P. and Turner, P. 2014. Felt seismicity associated with shale gas hydraulic fracturing: The first documented example in Europe. Geophysical Research Letters, v. 41, p.8308-8314.

De Barros, L., Cappa, F., Guglielmi, Y., Duboeuf, L. and Grasso, J.R. 2019. Energy of injection-induced seismicity predicted from in-situ experiments. Scientific Reports, v. 9, 4999.

Eaton, D., 2018. Passive seismic monitoring of induced seismicity: fundamental principles and application to energy technologies. Cambridge University Press.

Eaton, D.W. and Igonin, N., 2018. What controls the maximum magnitude of injection-induced earthquakes? The Leading Edge, v. 37(2), p.135-140.

Eaton, D.W., Igonin, N., Poulin, A., Weir, R., Zhang, H., Pellegrino, S. and Rodriguez, G. 2018. Induced Seismicity Characterization during Hydraulic-Fracture Monitoring with a Shallow-Wellbore Geophone Array and Broadband Sensors. Seismological Research Letters, v. 89, p.1641-1651.

Ellsworth, W. L. 2013. Injection-induced earthquakes, Science, v. 341, doi:10.1126/science.1225942.

Farrugia, J. J., Atkinson, G.M. and Molnar, S. 2017. Validation of 1D earthquake site characterization methods with observed earthquake site amplification in Alberta, Canada, Bulletin of Seismological Society of America, v. 108, p. 291-308.

Galis, M., Ampuero, J.P., Mai, P.M. and Cappa, F. 2017. Induced seismicity provides insight into why earthquake ruptures stop. Science Advances, v. 3, eaap7528.

Hotovec-Ellis, A.J., and Jeffries, C. 2016. Near real-time detection, clustering, and analysis of repeating earthquakes: Application to Mount St. Helens and Redoubt volcanoes. Presented at Seismological Society of America Annual Meeting, Reno, Nevada, 20 April.

Jia, S.Q., Eaton, D.W. and Wong, R.C. 2018. Stress inversion of shear-tensile focal mechanisms with application to hydraulic fracture monitoring. Geophysical Journal International, v. 215, p.546-563.

Kao, H., Hyndman, R., Jiang, Y., Visser, R., Smith, B., Babaie Mahani, A., Leonard, L., Ghofrani, H. and He, J. 2018. Induced seismicity in Western Canada linked to tectonic strain rate: Implications for regional seismic hazard. Geophysical Research Letters, v. 45, p.11-14.

Lei, X., Wang, Z. and Su, J. 2019. The December 2018 ML 5.7 and January 2019 ML 5.3 Earthquakes in South Sichuan Basin Induced by Shale Gas Hydraulic Fracturing. Seismological Research Letters, v. 90, p.1099-1110.

Mahani, A.B., Schultz, R., Kao, H., Walker, D., Johnson, J. and Salas, C. 2017. Fluid injection and seismic activity in the northern Montney play, British Columbia, Canada, with special reference to the 17 August 2015 Mw 4.6 induced earthquake. Bulletin of the Seismological Society of America, v. 107, p.542-552.

Mahani, A.B., Kao, H., Atkinson, G.M., Assatourians, K., Addo, K. and Liu, Y. 2019. Ground motion characteristics of the November 30, 2018 injection-induced earthquake sequence in northeast British Columbia, Canada, Seismological Research Letters, in review.

Novakovic, M., Atkinson, G. M. and Assatourians, K. 2018. Empirically calibrated ground-motion prediction equation for Oklahoma, Bulletin of Seismological Society of America, v. 108, p. 2444-2461.

Novakovic, M., Atkinson, G. M., Assatourians, K. and Gu, Y. (2019). Empirically calibrated ground-motion prediction equation for Alberta, Bulletin of Seismological Society of America, in review.

Petersen, M.D., Mueller, C.S., Moschetti, M.P., Hoover, S.M., Shumway, A.M., McNamara, D.E., Williams, R.A., Llenos, A.L., Ellsworth, W.L., Michael, A.J. and Rubinstein, J.L. 2017. One-year seismic-hazard forecast for the central and eastern United States from induced and natural earthquakes. Seismological Research Letters, v. 88, p.772-783.

Price, R.A. 1990. Cordilleran tectonics and the evolution of the Western Canada Sedimentary Basin. In: Geological Atlas of the Western Canada Sedimentary Basin. G.D. Mossop and I. Shetsen (comps.). Calgary, Canadian Society of Petroleum Geologists and Alberta Research Council, chapter 2.

Richards, B.C., Barclay, J.E., Bryan, D., Hartling, A., Henderson, C.M. and Hinds, R.C. 1990. Carboniferous strata of the Western Canada sedimentary basin. G.D. Mossop and I. Shetsen (comps.). Calgary, Canadian Society of Petroleum Geologists and Alberta Research Council, chapter 14.

Rodriguez-Pradilla, G. and Eaton, D. 2019. Near-field ground-motion analysis of a seismicity sequence induced by a hydraulic-fracturing in western Canada. Bulletin of Seismological Society of America, in review.

Rubinstein, J.L. and Mahani, A.B. 2015. Myths and facts on wastewater injection, hydraulic fracturing, enhanced oil recovery, and induced seismicity. Seismological Research Letters, v. 86, p.1060-1067.

Schultz, R., Wang, R., Gu, Y.J., Haug, K. and Atkinson, G.M., 2017. A seismological overview of the induced earthquakes in the Duvernay play near Fox Creek, Alberta. Journal of Geophysical Research: Solid Earth, v. 122, p.492-505.

Skoumal, R.J., Brudzinski, M.R. and Currie, B.S. 2015. Earthquakes induced by hydraulic fracturing in Poland Township, Ohio. Bulletin of the Seismological Society of America, v. 105, p.189-197.

Walsh III, F.R. and Zoback, M.D. 2016. Probabilistic assessment of potential fault slip related to injection-induced earthquakes: Application to north-central Oklahoma, USA. Geology, v. 44, p.991-994.